Ice-templated freeze-dried cryogels from tunicate cellulose nanocrystals with high specific surface area and anisotropic morphological and mechanical properties

Clémentine Darpentigny, Sonia Molina-Boisseau, Guillaume Nonglaton, Julien Bras, Bruno Jean

▶ **To cite this version:**

Clémentine Darpentigny, Sonia Molina-Boisseau, Guillaume Nonglaton, Julien Bras, Bruno Jean. Ice-templated freeze-dried cryogels from tunicate cellulose nanocrystals with high specific surface area and anisotropic morphological and mechanical properties. Cellulose, 2019, 27, pp.233-247. 10.1007/s10570-019-02772-8 . hal-02350610

HAL Id: hal-02350610
https://hal.science/hal-02350610

Submitted on 10 Sep 2024

HAL is a multi-disciplinary open access archive for the deposit and dissemination of scientific research documents, whether they are published or not. The documents may come from teaching and research institutions in France or abroad, or from public or private research centers.

L'archive ouverte pluridisciplinaire **HAL**, est destinée au dépôt et à la diffusion de documents scientifiques de niveau recherche, publiés ou non, émanant des établissements d'enseignement et de recherche français ou étrangers, des laboratoires publics ou privés.

Ice-templated freeze-dried cryogels from tunicate cellulose nanocrystals with high specific surface area and anisotropic morphological and mechanical properties

Clémentine DARPENTIGNY,[1,2,3] Sonia BOISSEAU,[1] Guillaume NONGLATON,[3] Julien BRAS[2] and Bruno JEAN*[,1]

[1]Univ. Grenoble Alpes, CNRS, CERMAV, 38000 Grenoble, France.
[2]Univ. Grenoble Alpes, CNRS, Grenoble INP, LGP2, F-38000 Grenoble, France
[3]Univ. Grenoble Alpes, CEA, LETI, DTBS, L2CB, F-38000 Grenoble, France
Corresponding author: bruno.jean@cermav.cnrs.fr + 33 (0)4 76 03 76 11

Abstract

High aspect ratio cellulose nanocrystals (CNCs) extracted from tunicate were used to create so-called cryogels from an ice-templating directional freeze-drying process. The structure of the resulting solid foam was investigated at the micro- and nanoscales by scanning electron microscopy and nitrogen adsorption measurements were used to extract the specific surface area. The mechanical properties were probed by compression tests. To highlight the specificities of tunicate CNC-based cryogels, results were compared with the one obtained from two other types of nanocellulose, namely cellulose nanofibrils (CNFs) from wood and cellulose nanocrystals (CNCs) from cotton, which exhibit different dimensions, aspect ratio, flexibility and crystallinity. While CNF- and cotton CNC-based cryogels exhibited a classical morphology characterized by a sheet-like structure, a particular honeycomb organization with individual particles was obtained in the case of tunicate CNC cryogels. The latter cryogels presented a very high specific surface area of about 122 m^2/g, which is unexpected for foams prepared from a water-based process and much higher than what was obtained for CNF and cotton CNC cryogels (25 and 4 m^2/g, respectively). High mechanical resistance and stiffness were also obtained with such tunicate CNC cryogels. These results are explained by the high crystallinity, aspect ratio and rigidity of the tunicate CNCs combined with the particular honeycomb architecture of the cryogel.

Keywords:

cryogel, freeze-drying, nanocellulose, tunicate CNCs

Abbreviations:

CNFs: cellulose nanofibrils

CNCs: cellulose nanocrystals

SEM: scanning electron microscopy

TEM: transmission electron microscopy

BET: Brunauer, Emmett, Teller

DLS: dynamic light scattering

NMR: nuclear magnetic resonance

NLDFT: nonlocal density functional theory

AFM: atomic force microscopy

Introduction

During the last decade, there has been increasing interest for nanoscale celluloses which can be extracted from plants, bacteria, fungi, algae and one marine animal, tunicate (Sacui et al. 2014), for which cellulose is present in the epidermal layer (Klemm et al. 2018). Two main types of nanocelluloses are classically described (Klemm et al. 2011; Dufresne 2012): cellulose nanofibrils (CNFs) and cellulose nanocrystals (CNCs). CNFs are a few micrometers long and 5 to 60 nm in diameter fibrils (Klemm et al. 2011; Lavoine et al. 2012; Nechyporchuk et al. 2016) comprising amorphous and crystalline regions leading to flexibility and possible entanglements. They are most commonly produced from a combination of a chemical or enzymatic pre-treatment followed by mechanical disintegration. CNCs are rigid rod-shaped particles usually produced from the acid hydrolysis of any cellulose source. They have dimensions of 100 nm to a few µm in length, and 4 to 70 nm in cross-section (Habibi et al. 2010; Klemm et al. 2011; Trache et al. 2017), which depend on the cellulose source and, to a lesser extent, on the hydrolysis conditions (Chauve et al. 2014). Owing to an extended range of properties (lightweight, natural abundance and renewable origin, biocompatibility, mechanical strength, tailorable surface chemistry), nanocelluloses are ideal building blocks for a wide range of applications (Abitbol et al. 2016) such as photonics (CNC chiral nematic properties for the production of iridescent films), nanocomposites (Wei et al. 2014), paper and packaging (Bardet and Bras 2013), electronics (Hoeng et al. 2016), biomedical applications (Jorfi and Foster 2015), or as rheology modifiers for cosmetics, paintings, etc.

Specifically, among the different nanocellulose-based materials and as discussed in recent reviews (Lavoine and Bergström 2017; De France et al. 2017), foams represent a very interesting category, which allows targeting a wide range of applications. Low-density materials with very high specific surface areas and a tunable architecture can be produced and these biosourced solid foams are able to compete with fragile inorganic aerogels.

These porous structures can be obtained from different processes. Solvent removal and formation of pores can be achieved by freeze-drying of the nanocellulose suspension with or without prior solvent exchange. Alternatively, supercritical conditions can be used, leading to a more fibrillary structure. Although both resulting structures are sometimes called “aerogels”, for a better understanding of the process accomplished and because the final structures are very different, the materials produced here via a freeze-drying process will be called “cryogels”. Solvent exchange of the nanocellulose suspensions from water to another solvent (commonly *tert*-butyl alcohol, *t*-BuOH) has been used to increase the specific surface area of the prepared porous materials. For example, Sehaqui et al. (2011) obtained CNF-cryogels with a surface area of 153 m^2/g that increased to 249 m^2/g after solvent exchange with *t*-BuOH. Similar results have also been reported by Fumagalli et al. (2013)b who discussed the influence of the water/*t*-BuOH ratio on the CNF cryogels morphology. Alternatively, a spray freeze-drying technique (Jiménez-Saelices et al. 2017) has been developed to prepare nanocellulose cryogels with reduced pore size and specific surface area of 100 m^2/g for insulating applications.

Despite the potential benefits that could be expected from these near-perfect high aspect ratio nanocrystals, the preparation of tunicate CNC (tuCNC) cryogels is poorly documented. Indeed, only Ishida et al. very briefly reported on the use of tuCNCs to prepare solid foams by freeze-drying with or without prior solvent exchange with *t*-BuOH (Ishida et al. 2004), while other authors reported the use of tuCNCs in the design of composite cryogels in combination with clay, polyvinylalcohol or polyimide (Gawryla et al. 2009; Mueller et al. 2015; Nguyen et al. 2016). In the present work, we aim to investigate the potential specificities of pure tuCNC-based cryogels. Therefore, porous structures were produced from the initial aqueous suspensions by an ice-templating freeze-drying procedure and the structural and physical properties of the resulting tuCNC-based materials were measured. Additionally, cryogels were also prepared with a similar process from commercial wood CNFs and CNCs derived from cotton (cCNCs) to investigate the influence of the starting nanocellulose type on the morphology and physical properties of the produced cryogels. This strategy aims at establishing the nanocellulose type-cryogels properties relationship to better adapt the nanocellulose source to a specific application. When of interest, properties of cryogels prepared from a suspension in water were compared to cryogels prepared from a suspension in *tert*-butyl alcohol.

Materials and methods

Materials

Chemicals

Hydrochloric acid (CAS Number: 7647-01-0, 37%), sodium hydroxide (≥97.0%, pellets, CAS number: 1310-73-2), sodium chlorite (technical grade, 80%, CAS number: 7758-19-2), sulfuric acid (98%, CAS number: 7664-93-9) were supplied by Sigma Aldrich and directly used as received and *tert*-butyl alcohol (≥99.0%, CAS number: 75-65-0) was purchased from Fisher Scientific and used without any further purification.

Tunicate CNCs

Mantles of tunicate (*Halocynthia roretzi*) were purified with 1N NaOH and 0.3% $NaClO_2$ treatments. Before hydrolysis, they were rinsed thoroughly, cut in small pieces and mixed with a blender. They were then partially dried over a Büchner membrane. Acid hydrolysis was carried out in 50 wt% sulfuric acid at 50°C during 20 hours under stirring. After hydrolysis, the acid was removed via centrifugation-dispersion cycles (centrifugation at 5000 to 7000 rpm during 30 min to 1 hour at 25°C) followed by dialysis at room temperature during 1 week. A suspension at 1.2 wt% was obtained.

Commercial CNFs

Cellulose nanofibrils from wood called Exilva® (type P) were provided by Borregaard at 2 wt% or 10 wt% solid content and were redispersed at 1 wt% solid content in distilled water using an Ultra Turrax IKA T25 stirrer at room temperature at 8 000 rpm during 5 minutes before use. The hemicellulose content was measured through alditol acetates preparation for monosaccharide analysis according to the procedure described by Blakeney et al (Blakeney et al., 1983) followed by analysis by GC-MS (Agilent GC6850-MS5975) using injection on a SP 2380 column (Supelco) with helium as carrier gas (1.1 $ml.min^{-1}$). A hemicellulose content of 2.8 % was obtained.

Cotton CNCs

Cotton linters from Buckeye Cellulose Corporation were cut in small pieces and mixed with a blender. Acid hydrolysis was carried out in 65 wt% sulfuric acid at 60°C during 30 min under mechanical stirring according to the method described by Revol et al. (1992). The acid was removed via centrifugation-dispersion cycles (centrifugation at 20000g for 30 minutes) followed by dialysis against distilled water until the conductivity reached the value of deionized water. The suspension was then ultra-sonicated using a Branson sonifier during 4 min in an ice-bath to prevent any temperature increase. The suspension was then filtered through a 1 µm Whatman membrane with a Sartorius filtration equipment to remove large aggregates. A suspension at 2.2 wt% was finally obtained.

Sample preparation

Solvent exchange

Nanocellulose particles were solvent exchange via centrifugation-dispersion cycles. A suspension of nanocellulose was centrifuged at 11200 rpm during 30 minutes at room temperature. The supernatant was discarded and the pellet was redispersed in tert-butyl alcohol at 30°C with Ultra Turrax IKA T25 stirrer at highest speed. Following centrifugations took place at 30°C to avoid freezing of tert-butyl alcohol. Four cycles of centrifugation-dispersion were necessary and the last pellet was dispersed in t-BuOH/H_2O 80:20 (V/V). For cotton CNCs, the addition of salt was necessary to increase the first centrifugation efficiency.

Freeze-drying

Nanocellulose cryogels were prepared from freeze-drying in a Cryotec® shelves freeze-drier. The nanocellulose suspension at specific solid content was poured in polystyrene cylindrical molds where the suspension was in direct contact with the freeze-drier shelves at -50°C. Directional freezing occurred at -50°C for 2 hours. The average freezing rate was of -10°C.min^{-1} and differences between the bottom and top part of the cryogel were observed, with a faster freezing rate occurring at the bottom than at the top. The primary freeze-drying step took place at 0.1 mbar with increasing temperature from -50°C to 20°C in 24 hours. It was followed by a secondary freeze-drying step at 20°C and 0.01 mbar for 30 minutes, after which cryogels were recovered. They were stored in a nitrogen cabinet to avoid humidity uptake.

Characterizations

Elemental analysis

C, O, H, and S elemental analysis was carried out by Institut des Sciences Analytiques (UMR 5280, Villeurbanne) on freeze-dried samples. At least duplicates were performed.

Dynamic light scattering

A suspension of nanocellulose at 0.1 %, was analyzed in a temperature-controlled chamber at 20 °C with a Malvern NanoZS instrument equipped with a 2 mW HeNe laser at a wavelength of 632.8 nm and detection was performed at an angle of 173°. Data analysis was performed with the multiple narrow mode algorithm from Malvern DTS software and the reported hydrodynamic diameter was averaged from 3 measurements of 15 runs each.

Titration

CNCs were prepared from sulfuric acid hydrolysis and their surface chemistry present OSO_3^- groups. A suspension of CNCs containing about 0.1 g dry CNCs was titrated at least twice with 0.01 M NaOH in order to evaluate the sulfur content. The degree of substitution was calculated from the following formula:

$$DS = \frac{V_{eq} x\ C_{NaOH}\ x\ M_{mean}}{m_{cellulose}}$$

$$M_{mean} = \frac{162}{1 - 80\ x(^{V_{eq}\ x\ C_{NaOH}}/_{m_{cellulose}})}$$

$$Sulfur\ amount = \frac{32\ x\ DS}{M_{mean}}$$

Where V_{eq} is the volume in mL of NaOH necessary for the titration of the CNC suspension, C_{NaOH} the concentration of NaOH for the titration is of 0.01M, M_{mean} is the mean molecular weight, $m_{cellulose}$ is the mass of titrated CNCs in g.

Cellulose nanofibrils nanoscale and microscale properties

The nanoscale and microscale particles fractions were evaluated by determining the homogeneity and the nano-sized fraction as explained in a quality index specifically developed for cellulose nanofibrils (Desmaisons et al. 2017). The microscopic part of the suspension was characterized from optical images obtained from 0.1% diluted suspensions. CNFs were sorted into three classes of dimensions: lower than 5 µm, from 5 to 10 µm and larger than 10 µm. Homogeneity was defined as the highest percentage of CNFs in any of the three dimensions' classes.

The nanoscale particles were also isolated from the CNF suspension after centrifugation of a 0.02% suspension at 1000 rpm during 15 minutes (Naderi et al. 2015). The supernatant was recovered and considered to be composed of nanoscale particles only. At least triplicates were performed.

The nanoscale fraction (%) is defined as $\frac{Concentration\ after\ centrifugation\ (wt\%)}{Concentration\ before\ centrifugation\ (wt\%)}\ x\ 100$

NMR analysis

^{13}C solid-state NMR spectra were recorded with a Bruker Avance DSX 400 MHz spectrometer, in a cross-polarization and magic angle spinning conditions (CP-MAS). The ^{13}C radio frequency field strength was obtained by matching the Hartman–Hahn conditions at 60 kHz. The spinning speed was

12000 Hz, the operating condition was set at 100.6 MHz and a minimum number of 10 000 scans were acquired with a contact time and recycle delay, respectively, of 2 ms and 2 s representing standard conditions. The acquisition time was set at 35 ms and the sweep width at 29 400 Hz. Spectra were corrected with the scaling factor obtained from a reference spectrum of glycine. The spectra were normalized with cellulose C1 peak at 100 to 110 ppm. Crystallinity was calculated from the integration of the crystalline (87 to 93 ppm) and amorphous (80 to 87 ppm) form of carbon C4.

Electron microscopy

The cellulose nanocrystal suspensions diluted 100 to 1000 times were observed with a Philips CM200 CRYO transmission electron microscope (TEM) operating at 80 kV. One drop of suspension was deposited on a carbon grid and excess liquid was removed. A 2% uranyl acetate stain was deposited on top of the samples, excess liquid was removed after 2 minutes and the sample was allowed to dry before observation.

Nanocellulose cryogels images were recorded with a FEI Quanta 250 scanning electron microscope (SEM) equipped with a field emission gun and operating at 2 kV, after sample coating with gold/palladium. At least ten images were recorded and the most representative were selected for discussion.

Atomic force microscopy (AFM)

Cellulose nanocrystal suspensions were diluted to 10^{-4} wt% and a drop was deposited on cleaved mica plate. The plate was left to dry overnight at room temperature. Analysis of the nanoparticles was carried out using a Dimension icon® atomic force microscope (Bruker, USA) in tapping mode with a silicon cantilever (OTESPA, Bruker, USA). At least 10 images were recorded and used for image treatment.

Image treatment

Particle sizes were measured from electron, optical and atomic force microscopy images using the ImageJ software. Reported average values of length and width correspond to at least 150 measurements.

Pore sizes of large pores (> 1µm) were measured from SEM images at magnifications from 200 to 1000 times. At least 100 replicates were recorded and pore size distribution was analyzed.

Density and porosity

The volume of the produced cryogels was determined from height and diameter measurements using a digital caliper. The density is given as the mass of cryogel for a given volume and an average

value of ten measurements was taken. The porosity, *P*, was calculated from the following equation: $P\ (\%) = (1 - \frac{\rho}{\rho_c}) \times 100$, where ρ the density of the cryogel and ρ_c the density of cellulose (1.60 g.cm^{-3})

Nitrogen adsorption

Specific surface area and pore size distribution were obtained using a Micromeritics ASAP 2420 Surface Area and Porosity Analyzer. Cryogels samples (around 100 mg) were degassed at 105°C during at least 12 hours. Analysis was performed with nitrogen adsorption and desorption at -196°C, at relative pressures from 0.01 to 0.03 for BET specific surface area and from 0.01 to 0.995 for pore size distribution. The specific surface area measurement was performed three times for each sample and for a given set of parameters two different batches were characterized. The specific surface area was calculated by assuming that nitrogen is adsorbed at the surface of the sample as a monolayer.

A nonlocal density functional theory (NLDFT) method was applied to obtain the pore size distribution of cryogels after pore geometry adjustment (Ravikovitch and Neimark 2001). The MicroActive software was used for the calculations.

Compression test

Compression tests were performed on a Shimadzu (autograph) AGS-X with load cell capacities of 20 N and 500 N (depending on the cryogel resistance) at 24°C and 50 (± 3) % relative humidity after at least 24 hours stabilization storage of cryogel in same conditions. Cryogels of cylindrical shape of 15 mm in diameter and 20 to 30 mm in height were compressed at 1 mm/min. Triplicates were performed. The compression moduli were calculated in the elastic region at strains (± 2.5%) corresponding to half the strain of the beginning of the plateau region.

Results and Discussion

Nanocellulose morphology and properties

Cellulose nanocrystal and cellulose nanofibril suspensions exhibit very different macroscopic features, as shown in the insets in **Fig.1**. For both types of CNCs, the preparation yields homogeneous and stable colloidal suspensions with a low viscosity. In the case of tunicate, some temporary iridescence can be observed when shearing is applied, due to the easy alignment of these high aspect ratio particles. The CNF suspensions appear more viscous, gel-like and non-transparent due to entanglements between the very long objects and the presence of poorly disaggregated elements. Characterization of cellulose nanomaterials is still a challenge and requires adapted technique or specific preparations as recently reviewed by the community (Foster et al. 2018). To investigate the

particles morphology, TEM images were acquired and are shown in **Fig.1**. Cotton CNCs have a rod-like structure with a moderate aspect ratio and are often observed as bundles of 3 to 4 laterally associated elementary crystallites, which the acid hydrolysis did not separate. This is in agreement with previously reported data (Elazzouzi-Hafraoui et al. 2008). Tunicate CNCs exhibit a much higher aspect ratio and a needle-like structure, due to a higher crystallinity when compared to cotton. TuCNC production rather yields isolated elementary crystallites with a lower degree of polydispersity than cCNCs. Regarding CNF material, a much more heterogeneous morphology is observed when multiscale tools like optical microscopy, SEM and TEM are used. The finest fraction in the CNF sample observed by TEM appears as long and flexible fibrils with a varying degree of defibrillation. The particles sizes distributions are recorded in supplementary materials, in figure SM1.

Table 1 summarizes the intrinsic properties of the three types of nanocelluloses in terms of dimensions and crystallinity. Sizes and aspect ratio of the different nanoparticles were deduced from TEM and AFM images analysis. Cotton CNCs have an average length of 150 nm and an average width of 19 nm and a height of 8 nm, giving an aspect ratio of 14, in agreement with literature values (Elazzouzi-Hafraoui et al. 2009; Cherhal et al. 2015). Tunicate CNCs have an average length of 1120 nm and a width of about 21 nm on average and a height of 12 nm giving an aspect ratio of 63, which is much bigger than the value for cCNCs. Dynamic light scattering (DLS) was used to measure the hydrodynamic diameter of CNCs only, since this technique is not suitable for micrometer-sized CNFs. Values of 129 and 381 nm were obtained for cCNCs and tuCNCs, respectively. It has here to be recalled that these values do not correspond to the length nor to the cross-section of the particles but to the size of the sphere with the same diffusion coefficient as the considered particle.

CNFs are much longer and entangled flexible fibers, as the defibrillation process mainly separates the fibrils and reduce their length to a much lesser extent than the acid hydrolysis used to prepare CNCs. Disordered regions along the fibrils provide flexibility to the CNFs. The cellulose nanofibril suspension is heterogeneous in size with nano, micro, and macroscale dimensions and were evaluated with the recently defined quality index (Desmaisons et al. 2017). The homogeneity of the suspension was determined from optical microscopy images. The various measured dimensions are sorted into three classes of different sizes. The homogeneity was defined as the highest percentage of CNF sizes in a same class and was of 37%, expressing a great heterogeneity. The micron-sized class dimensions were measured from optical microscopy images and are of 9 µm in length and 0.9 µm in diameter, on average. The nanoscale components were analyzed after centrifugation of a highly diluted suspension without entangled particles. The quantity of nanofibrils is defined from the nano-sized fraction, and was equal to 34 % of the total suspension. The nano-sized fraction defines the part of nanoparticles in a suspension composed of nanofibrils and also CNF

aggregates and large objects. Their dimensions are estimated from electron microscopy images and objects with an average diameter of 25 nm and length higher than 1.7 µm are observed. It should be noted that the full length of individual nanofibrils can usually not be observed as they do not fit in the image size, therefore the aspect ratio of the cellulose nanofibrils is higher than 68.

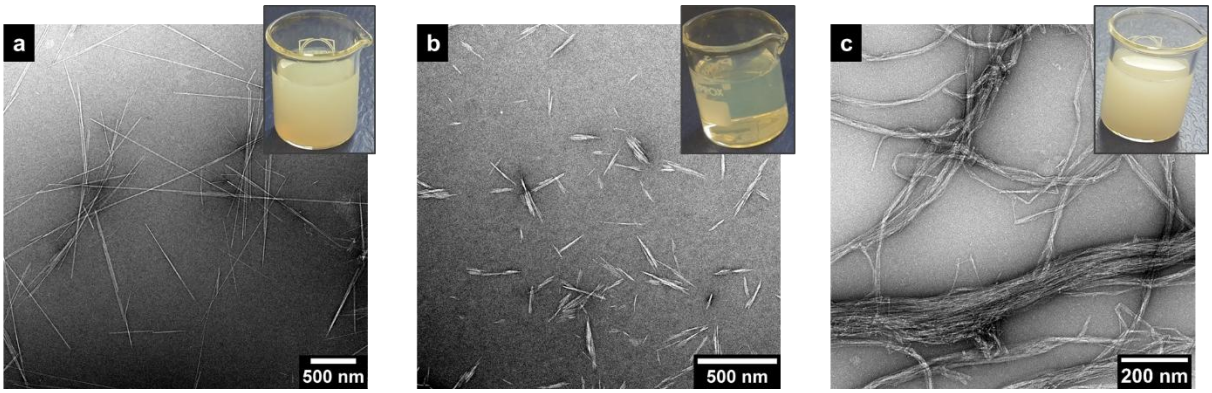

Fig.1 TEM images and corresponding photographs of suspensions of tunicate CNCs (a), cotton CNCs (b), and CNFs (c).

Table 1 Nanocellulose dimensions and crystallinity. [a] Extracted form TEM micrographs. [b] Obtained from AFM measurements. [c]Calculated from the ratio of the length to the average cross-section dimension. [d]Obtained from DLS measurements. [e]Assesed from ^{13}C NMR measurements.

	tuCNCs	cCNCs	CNFs (nanosize fraction)
length[a] (nm)	1120 ± 473	150 ± 56	> 1702
width[a] (nm)	21 ± 6	19 ± 8	25 ± 14
height[b] (nm)	12	8	n/a
Aspect ratio[c]	63	14	> 68
Hydrodynamic diameter[d] (nm)	381 ± 172	129 ± 76	n/a
Crystallinity[e]	94 %	75 %	49 %

The crystallinity was assessed by ^{13}C NMR analysis. It is commonly calculated from the signals related to carbon C4, which appears at 83 ppm in its amorphous form and at 86 ppm in its crystalline form. Cotton CNCs have a degree of crystallinity of 75 %. Tunicate CNCs exhibit near-perfect crystallinity with a degree of crystallinity of 94 %. This is explained by the high degree of crystallinity of tunicate cellulose that plays a structural role for this marine organism, although this value seems to vary a lot with the tunicate species (Zhao and Li 2014). CNFs appears to be semi-crystalline with 49 % crystallinity. This is explained by the low crystallinity of cellulose in wood and the extraction process used which does not imply acid hydrolysis but enzymatic treatment (commonly

endoglucanase enzymes attack parts of the cellulose) and a mechanical treatment to defibrillate the fibrils.

Cryogels morphology and structure

The morphological and structural properties of nanocellulose cryogels obtained from ice-templating and freeze-drying were investigated. The macro- and microscales morphologies are shown in **Fig.2**. The cylindrical shaped cryogels appear as non-transparent white foams. Cotton CNC cryogels are crumbly and brittle, however, CNF and tuCNC cryogels have a better holding and more homogeneous structure. It is clearly possible to observe an upright orientation of the structure for tuCNC cryogels at the macroscopic scale (**Fig.2a**)

Firstly, for each nanocellulose cryogel, a flat and sheet-like structure seems to be observed. However, it is worth noting that when walls of tuCNC cryogels are zoomed-in, a fine organization emerges and appears as “interlaced” or “netted” sheets, with isolated nanoparticles as observed in **Fig3c**. On the contrary, cCNC and CNF cryogels sheets appear thick and dense. Tunicate CNC cryogels present a morphology similar to previously observed cross-linked short CNCs. Indeed, cross-linking appears to result in cryogels that do not present fully packed walls and with a microporosity as observed by Yang and Cranston (2014) and Osorio et al. (2018). Such results suggest that tunicate CNCs are naturally forming a network, whereas for cCNCs it is necessary to chemically cross-link the nanocrystals to obtain an analogous cryogel morphology.

The sheet-like structure is explained by the growth of ice-crystals during the freezing step that pushes the nanocellulose particles away and together. This was not observed when cryogels are obtained from a suspension of nanocellulose in *tert*-butyl alcohol (*t*-BuOH/H_2O, 80:20), which appear to have a finest and more fibrillary structure (Supplementary material, Figure SM2). Such a behavior has been observed before, for example by Jin et al. (2004) where they studied the effect of the solvent exchange on the final cryogel structure.

Cryogels prepared from tunicate CNCs are anisotropic and present a completely different architecture depending on whether the longitudinal section or the cross-section is considered, as shown in **Fig.3a** and **b**. An alveolar structure is observed for cross-section images, resulting from the growth of ice in a specific direction. The freezing is induced from the bottom part of the hydrogel that is in contact with the frozen shelf of the freeze-drier. Instead of growing in random directions, the crystals grow towards the upper part of the hydrogel. The high aspect ratio and great rigidity of the tunicate CNCs prevent the arbitrary expansion of water, hence favor the resulting honeycomb structure. Similar organization was observed for TEMPO-oxidized CNF cryogels by Chen et al. (2019) with honeycomb pores in the cross section and directional tunnels in the longitudinal section. Munier

et al. (2016) have observed orientation of the particles induced by unidirectional freezing, that leads to the formation of cellular structures, as observed here for tuCNC cryogels. They quantified the degree of orientation with X-ray diffraction and confirmed the highest orientation for freeze-casted cryogels compared to the freeze-crashing ones. The lower orientation of CNF than CNC cryogels is even more pronounced due to CNF flexibility and aggregates, the presence of which explains why very little orientation is observed for the ice-templated heterogeneous CNF suspensions.

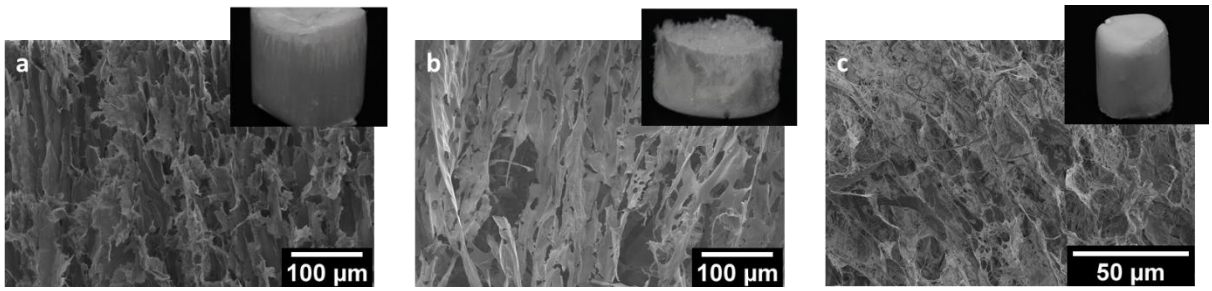

Fig.2 Longitudinal section SEM images of tunicate CNC (a), cotton CNC (b), CNF (c) cryogels prepared from a suspension in water.

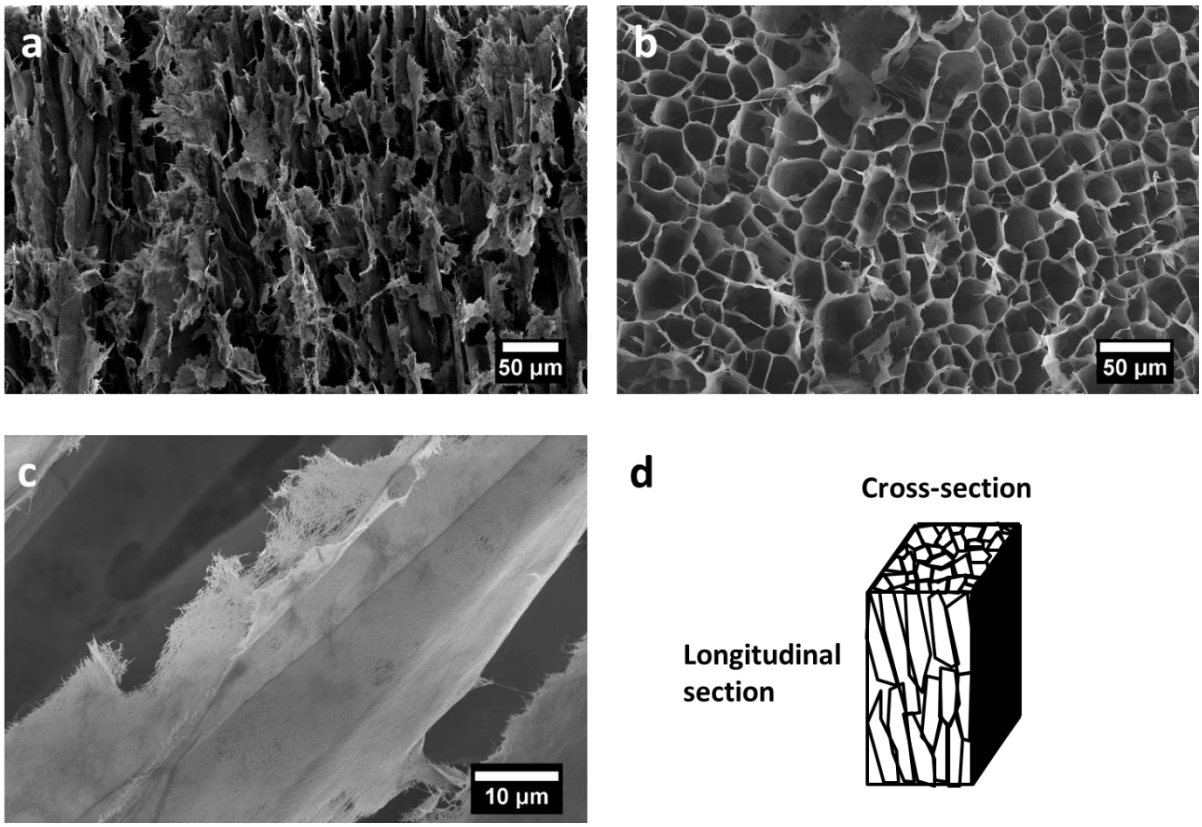

Fig.3 SEM images of tunicate CNC cryogels from a longitudinal section (a) and cross-section (b), zoomed-in image of tuCNC cryogels wall (c), cross and longitudinal section schematic representation (d).

Various properties, namely specific surface area, density and pore size of the prepared cryogels, are summarized in **Table 2**.

The value of density for tuCNC cryogels and CNF cryogels are close to 10 mg/cm^3, close to the initial concentration (1 wt%). This indicates that there is little shrinkage and pore collapse. However, the density measurement was not accurate for cCNC cryogels because of their very brittle behavior and an estimated value was reported here for this sample. The samples exhibit very high porosity, with calculated values of 99.3 (± 0.1) % for tuCNC cryogels and 99.4 % for CNF cryogels. For cotton CNC cryogels, a value of 99.3 (± 0.1) % of porosity was estimated, assuming that the cryogels exhibit between 0 and 33 % shrinkage.

The specific surface areas of each cryogel were determined from nitrogen adsorption and application of the Brunauer–Emmett–Teller (BET) theory, estimating the amount of nitrogen molecules adsorbed as a monolayer at the surface of the cryogels. Full adsorption and desorption isotherms were acquired and type IV isotherms, corresponding to mesoporous samples, were obtained according to IUPAC classification.

Cryogels prepared from cotton CNCs exhibit a very low specific surface area of 4 ± 2 m²/g, which is in the lower range compared to what has been published, with values of 17 m²/g observed for cotton CNC cryogels (Fumagalli et al. 2013), although few cryogels have been produced with sulfate half-ester CNCs using the freeze-drying process. CNF cryogels exhibit a specific surface area of 25 ± 2 m²/g, in fair agreement with results reported by Cervin et al. (2012) for CNF porous cryogels prepared under similar conditions. Such low specific surface area values are usually attributed to the growth of large ice crystals during the freezing step of the freeze-drying process, which pushes the nanocellulose elements towards the outer limits of the crystals, inducing their aggregation as sheets located between neighboring ice crystals. However, for tuCNC-based samples and despite the use of water-based suspensions, an unexpectedly high surface area of 122 ± 10 m²/g was measured. Such a high value would in fact have been expected for cryogels prepared from suspensions in *tert*-butyl alcohol. It has indeed been shown in literature that solvent exchange from water to tert-butyl alcohol is highly beneficial to a strong increase of the specific surface area of CNF or CNC-based cryogels up to 249 m^2/g (Sehaqui et al. 2011). While we could verify that such a solvent exchange results in a very significant increase of the specific surface area from 25 ± 2 to 97 ± 4 m²/g for CNF-based cryogels, in agreement with literature data (with surface areas after solvent exchange and freeze-drying twice higher than for regular cryogels (Jin et al. 2004)), only a slight increase to 150 ± 21 m²/g could be obtained for tuCNC-based cryogels prepared from suspensions in *tert*-butyl alcohol (Supplementary material Table SM1). This result emphasizes the very peculiar behavior of tuCNCs, which enable the

preparation of cryogels with high specific surface area directly from water-based suspensions. Surprisingly, using tunicate CNCs, Ishida et al. (2004) reported specific surface area values of 25 and 130 m^2/g for cryogels prepared by freeze-drying without solvent exchange and after solvent exchange with t-BuOH, respectively, but no details on the freeze-drying process or further characterizations were provided to allow for a deeper comparison.

The theoretical value of the specific surface area of isolated tuCNCs is of 165 m^2/g, considering average dimensions of 1120 x 21 x 12 nm^3 and a density of 1.6 $g.cm^{-3}$. This value is very close to the specific surface area obtained for tuCNC cryogels using the experimental nitrogen adsorption BET method. This suggests that almost every nanocrystal is individualized and contributes to the specific surface area. Such an hypothesis is supported by SEM observations (Fig.3a and c), which show that the tunicate nanocrystals forming the solid foam remain well separated and not aggregated as in the case of cCNC and CNF cryogels. This high degree of individualization of the particles in the final cryogel material enables to preserve the accessibility of the tuCNC surface. It has also to be noted that, even if not easily detected by TEM, thin particles with widths lower than 20 nm were not taken into account in the theoretical surface area calculation but would strongly contribute to it. The high specific surface area of tunicate CNC cryogels therefore arises from a distinct morphology resulting from the high rigidity and crystallinity of the tuCNCs, in addition to their high aspect ratio. This characteristic morphology limits the random growth of ice crystals. This behavior can tentatively be explained by the formation upon drying of a rigid yet sparse tuCNC network that was formed through the creation of a limited number of hydrogen bonds along the particle's long axis. This situation is reminiscent of the use of tuCNCs in nanocellulose/polymer layer-by-layer films, where the long and stiff tuCNCs allowed the formation of a "porous matchsticks pile", which led to strong antireflective properties, while the use of cCNCs rather resulted in very dense layers, preventing antireflection (Podsiadlo et al. 2007; Jean et al. 2008; Martin and Jean 2014).

The sulfur content was determined by conductometric titration and a value of 0.73 % was obtained for cCNCs. This method was not accurate for tuCNC sulfur amount determination as the amount is too low. Elemental analysis complements the titration results, with 0.61% S for cotton CNCs and a value inferior to 0.1 % for tunicate CNCs. The charge density being lower for tuCNCs compared to cCNCs, tuCNCs would be expected to be more aggregated. Therefore, the great individualization of the tuCNCs is not due to the surface charge present on the surface of the CNCs and must be explained with the intrinsic organization of cellulose inside the tunicate mantles and their high rigidity and crystallinity.

Table 2 Specific surface areas (SSA) calculated from BET method and average pore sizes measured from SEM images, for cryogels prepared from tunicate CNCs, cotton CNCs and CNFs from a suspension in water

	SSA (m^2/g)	Density ($mg.cm^{-3}$)	Average pore size (µm) [a]
tuCNCs	122 ± 10	11.5 ± 1.0	17.6 ± 5.7 *(cross-section)* 66.2 ± 30.4 *(longitudinal section)*
cCNCs	4 ± 2	10 *(estimated)*	8.7 ± 7.5
CNFs	25 ± 2	10.2 ± 0.2	17.8 ± 13.8

The pore sizes were determined from the treatment of SEM images and the resulting pore size distribution histograms are plotted in **Fig.4**. Because of their singular organization, the pore size of tunicate CNC cryogels were measured for both longitudinal and cross-section directions. They have an average diameter of 66 µm in the longitudinal section and 18 µm in cross-section. Cotton CNC cryogels have 9 µm pores. CNF cryogels have a mean pores diameter of 18 µm.

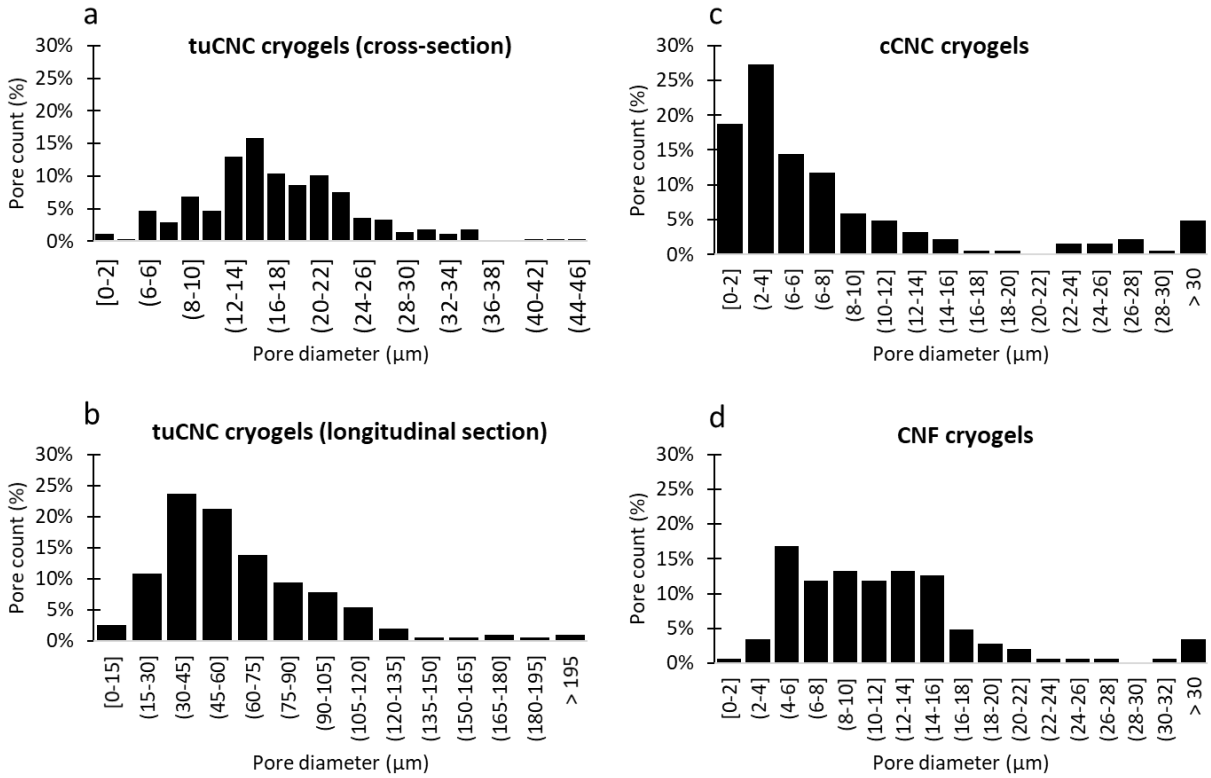

Fig.4 Pore size distribution extracted from SEM images of tunicate CNC (a: cross-section, b: longitudinal section), cotton CNC (c) and CNF (d) cryogels prepared from a suspension in water

In order to perform a multiscale pore size analysis, the mesoporosity was calculated from nitrogen adsorption and after applying nonlocal density functional theory (NLDFT) and adjusting the pore geometry. The pore size distributions are presented in supplementary material (Fig. SM4). However, as discussed by Rudaz et al. (2014), nitrogen adsorption technique only considers a very small portion of pores with width lower than 60 nm.

The combination of the two techniques brings to light the presence of both micron-sized pores and mesopores in each cryogel. Large pores, observed from microscopy images, are introduced during the freezing process and the pore size distribution profiles are very different for the three types of nanocellulose. The amount of small pores is influenced by the starting nanocellulose particles, as observed from nitrogen adsorption experiments. However, the distribution profiles of small pores are very similar, with analogous well-defined pore sizes observed for each structure. The pores of size inferior to 60 nm are resulting from contact point between the nanocellulose particles, as suggested by Robitzer et al. (2011).

Cryogels mechanical properties

Compression tests were carried out on the cylindrical shaped cryogels and the obtained stress-strain curves are shown in **Fig.5a**. In each case, two different regions are observed: the first part of

the curve corresponds to the elastic domain with a deformation below 10%-20 % depending on the cryogels and after a yield point the plastic region is reached. Martoïa et al. (2016) observed these typical regimes for CNF and TEMPO-oxidized CNF cryogels. At early stage of elastic deformation, bending of the pore walls was observed. After increasing strain, collapse and severe deformation of the pore occurs, as well as tearing. After 70% deformation (not represented here), the densification of the material occurs and the pores collapsed and packed together. These regimes are similarly observed here for tunicate CNC and CNF cryogels.

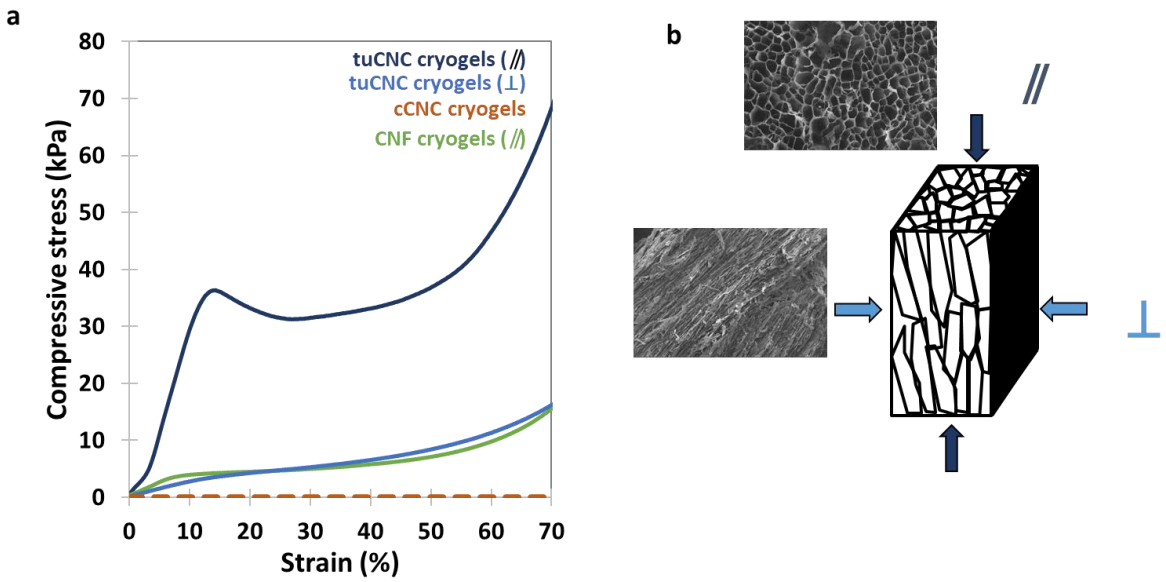

Fig.5 Stress-stress compression curves of tunicate CNC, cotton CNC and CNF cryogels (a). For tunicate CNC cryogels, measurements were carried out both parallel and perpendicular to the direction of freezing as illustrated in (b).

The modulus was calculated in the elastic region. Compression moduli and maximum stress at 70% deformation are summarized in **Table 3**. Cotton CNC cryogels were very fragile and crumbly, therefore cryogels with the appropriate shape could not be prepared and accurate compression curves could not be obtained. Compression was performed both parallel and perpendicular to the ice-templating direction, as presented in **Fig.5b** for tunicate CNC cryogels. The perpendicular direction corresponds to the longitudinal section compression and the parallel direction corresponds to the cross-section compression. CNF cryogels compression curves are presented for the compression direction parallel to the direction of freezing only due to the difficulty to cut cryogels with suitable and defined shape for compression testing in the perpendicular direction.

Table 3 Compression modulus, normalized modulus and maximum stress at 70% deformation for tuCNC and CNF cryogels.

Cryogel	Modulus (kPa)	Normalized modulus (kPa. mg^{-1}. cm^3)	Maximum stress at 70% deformation (kPa)

tuCNCs //	138 ± 44	12 ± 3.8	57 ± 9
tuCNCs ⊥	36 ± 13	3.1 ± 1.1	17 ± 3
cCNCs	*Not suitable*	*Not suitable*	*Not suitable*
CNFs //	28 ± 4	2.7 ± 0.4	17 ± 2

460

461 A striking difference is observed for the parallel compression curves of tuCNC and CNF cryogels.
462 While the compression modulus of CNF cryogels was of 28 kPa, a much higher value of 138 kPa was
463 measured for tuCNC cryogels. For the latter, a very clear region of pore collapse characterized by a
464 decrease of stress with increasing strain is observed from 15 to 25% of compression strain, followed
465 by a plateau and finally a steep rise after 55% strain reflecting a densification of the material. The
466 cryogel morphology, with directional and elongated pores, can explain the high resistance of the
467 material until a certain degree of compression after which the pores collapse. This compressive
468 behavior is specific to lattice materials, for which the plateau region is due to elastic buckling (Ashby
469 2006). These materials are also said to present a "cellular" organization and are designed to prepare
470 stiff and resistant materials for applications that require a light material or when as little material as
471 possible is to be used. The observed mechanical behavior is qualitatively in close agreement with
472 results recently reported by Chen et al. (2019) on TEMPO-oxidized CNF aerogels exhibiting the same
473 type of structural anisotropy.

474 The tunicate CNC morphology and properties, *i.e.* their high aspect ratio, high crystallinity and
475 rigidity, are also responsible for the stiffness of the cryogels. When tuCNC cryogels are compressed in
476 the perpendicular direction, the compression modulus drops to 36 kPa, and the curve profile and
477 modulus are similar to those of parallel CNF cryogels. Martoïa et al. (2016) observed that the
478 compression modulus of TEMPO-oxidized CNFs with high aspect ratio was higher than for enzymatic
479 heterogeneous CNFs. They studied the effect of the CNF type and morphology on the stuctural
480 organization and observed that TEMPO-oxidized CNFs lead to more regular anisotropic pore
481 stuctures with unimodal size. However, CNF suspensions that are more heterogeneous lead to
482 reduced anisotropy. By comparing classical freezing to sorbet freezing, the role of a cellular
483 organisation on the increase of mechanical properties was emphasized. The effect of the
484 nanocellulose morphology on the mechanical properties was also investigated by Kriechbaum et al.
485 (2018). They especially studied the effect of the energy consumption during CNF production on the
486 CNF diameters and on the compression modulus of the prepared cryogels. A decrease in the
487 diameter of the CNFs resulted in an increase of compression modulus (26-fold), until a plateau is

reached. The authors suggested that when the amount of CNFs of small diameters increases, more bonds and entanglements are formed which increases the mechanical properties. Such a mechanism could account for the higher moduli measured for tuCNCs than for CNFs since tuCNCs only comprise thin rods while CNFs also contain thicker objects, which were not defibrillated.

Compression moduli have been normalized with the cryogel density. Mechanical behavior reported for CNF materials are similar to what is observed in this paper, with normalized moduli of 2.5 $kPa.mg^{-1}.cm^3$ (Sehaqui et al. 2011), 3.8 and 6.3 $kPa.mg^{-1}.cm^3$ (Gupta et al. 2018). For TEMPO-oxidized CNF cryogels moduli of 6.7 and 5.9 $kPa.mg^{-1}.cm^3$ were reported by Jiang and Hsieh (2014) and Martoïa et al. (2016). Fewer literature is available on the mechanical properties of CNC-only cryogels. A modulus of 9.4 $kPa.mg^{-1}.cm^3$ was obtained by Osorio et al. (2018) for cross-linked CNC cryo-templated aerogels, obtained by supercritical drying. Tripathi et al. (2019) reported the highest values of compression modulus with values up to 21.5 $kPa.mg^{-1}.cm^3$ for CNC aerogels. However, the materials differ from the tuCNC cryogels presented in this study because they are prepared from supercritical drying and have 10-fold higher densities (171 $mg.cm^{-3}$).

A power-law relationship has been described by Gibson and Ashby (1999) for cellular materials. The compression modulus plotted as a function of the relative cryogel density gives a curve of the type $E \propto (\rho/ \rho_{cellulose})^m$. The scaling exponent, *m*, was described to be dependent on the type of foam (Budtova 2019). Cryogels at various densities were prepared and the moduli calculated from the compression stress-strain curves. **Fig.6** illustates the power-law relationship between the modulus and the density for tuCNC and CNF cryogels.

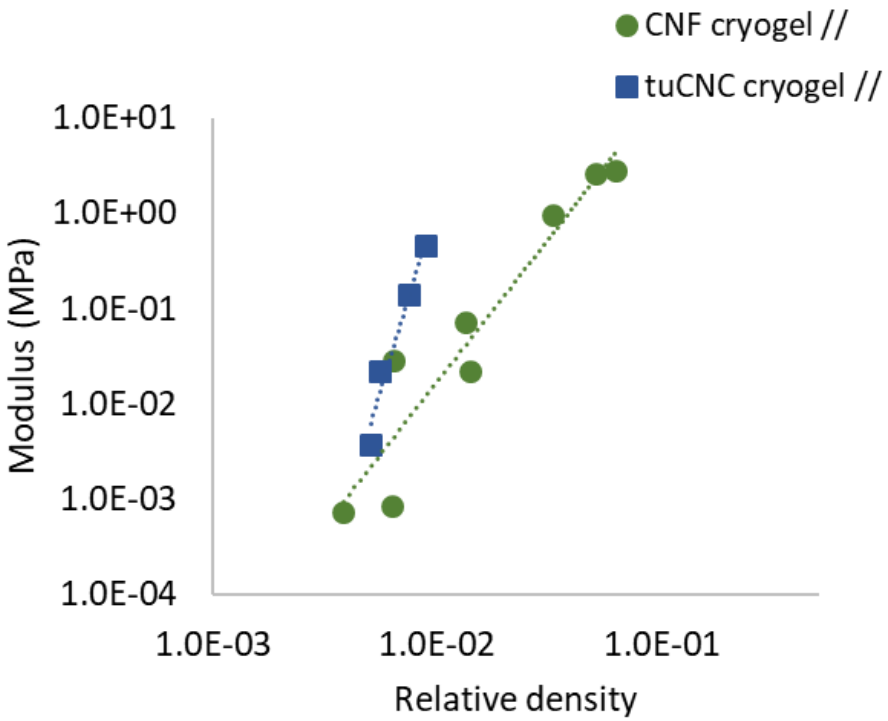

508

509 **Fig.6** Compression modulus of tuCNC and CNF cryogels as a function of relative density.

510 A scaling exponent of 3 was observed for CNF cryogel, close to was has been previously
511 described for enzymatic CNF cryogels by Martoïa et al. (2016), who reported a scaling exponent of
512 3.1. However, for tuCNC cryogels, a value of 7.8 was unexpectedly obtained. As mentioned by Zhao
513 et al. (2018) in their review, the scaling exponent of biopolymer foams usually varies from 1 to 4. At
514 increasing solid content, the cellulose nanocrystals present more contact points and interactions and
515 this results in very high mechanical properties. Although the experiment was performed on a small
516 range of densities, the mechanical behavior of tuCNC cryogels is outstanding and promising for the
517 design of highly resistant porous materials.

518 **Conclusion**

519 In this work, different types of nanocelluloses obtained from different sources and different
520 extraction processes were compared. Cellulose nanocrystals from cotton and tunicate both have high
521 crystallinities and tuCNCs present an aspect ratio 5 times higher than cCNCs. Semi-crystalline
522 cellulose nanofibrils are derived from wood sources. From these different cellulose nanoparticles,
523 cryogels were prepared by an ice-templating freeze-drying process, and morphological observations
524 were made on the lightweight and highly porous materials. While CNF and cotton CNC cryogels
525 displayed a classical sheet-like structure and a random organization, tunicate CNC cryogels revealed
526 an eminently organized honeycomb structure.

The nitrogen adsorption analysis demonstrates the very high specific surface area of 122 m^2/g for the tunicate CNC cryogel prepared directly from a water suspension. This result is particularly interesting as such high values of specific surface area are usually obtained after time-consuming solvent exchange steps. In a second step, the mechanical properties of the cryogels were assessed by compression experiments. Cotton CNC cryogels were too weak to produce cryogels of the desired shape for compression tests. CNF cryogels displayed a weak resistance and a low Young's modulus of 28 kPa. Tunicate CNC cryogels displayed a different behavior depending on the direction of compression. This anisotropic behavior had not been observed before. Indeed, while tuCNC cryogels present a similar compressive behavior to CNF cryogel for perpendicular compression, when the compression direction was out of plane they displayed a high mechanical resistance to compression and a Young's modulus of 138 kPa. This result is remarkable for a 1% solid content material. Such unexpected and outstanding properties of high specific surface area and mechanical properties are explained by the specific honeycomb configuration of the tuCNC cryogel, itself explained by the directional freezing process and the near-perfect crystallinity and high aspect ratio of the tunicate cellulose nanocrystals. This work illustrates how the near-perfect tuCNCs can be used to yield materials with enhanced and new properties.

Acknowledgements

This work was supported by a grant from Labex ARCANE and CBH-EUR-GS (ANR-17-EURE-0003) and supported by the "Investissement d'avenir" program Glyco@Alps (ANR-15-IDEX-02). The authors acknowledge the Borregaard company for providing CNF materials and thank Jean-Luc Putaux and Christine Lancelon-Pin (CERMAV, Grenoble) for the electron microscopy images and Stéphanie Pradeau (CERMAV, Grenoble) for the measurement of the hemicellulose content in the CNF material. LGP2 is part of the LabEx Tec 21 (Investissements d'Avenir—Grant Agreement No. ANR-11-LABX-0030) and of PolyNat Carnot Institute (Investissements d'Avenir—Grant Agreement No. ANR-16-CARN-0025-01). CD would like to thank Laurent Orgéas (3SR laboratory, Grenoble) for fruitful discussion.

References

Abitbol T, Rivkin A, Cao Y, et al (2016) Nanocellulose, a tiny fiber with huge applications. Curr Opin Biotechnol 39:76–88. doi: 10.1016/j.copbio.2016.01.002

Ashby MF (2006) The properties of foams and lattices. Philos Trans R Soc Lond Math Phys Eng Sci 364:15–30. doi: 10.1098/rsta.2005.1678

559 Bardet R, Bras J (2013) Cellulose Nanofibers and Their Use in Paper Industry. In: Handbook of Green
560 Materials. WORLD SCIENTIFIC, pp 207–232

561 Blakeney AB, Harris PJ, Henry RJ, Stone BA (1983). A simple and rapid preparation of alditol
562 acetates for monosaccharide analysis. Carbohydr Res 113(2), 291-299. doi:
563 10.1016/0008-6215(83)88244-5.
564 Budtova T (2019) Cellulose II aerogels: a review. Cellulose 26:81–121. doi: 10.1007/s10570-018-2189-
565 1

566 Cervin NT, Aulin C, Larsson PT, Wågberg L (2012) Ultra porous nanocellulose aerogels as separation
567 medium for mixtures of oil/water liquids. Cellulose 19:401–410. doi: 10.1007/s10570-011-
568 9629-5

569 Chauve G, Fraschini C, Jean B (2014) Separation of Cellulose Nanocrystals. In: Materials and Energy.
570 WORLD SCIENTIFIC, Singapore, pp 73–87

571 Chen Y, Zhou L, Chen L, et al (2019) Anisotropic nanocellulose aerogels with ordered structures
572 fabricated by directional freeze-drying for fast liquid transport. Cellulose 26:6653–6667. doi:
573 10.1007/s10570-019-02557-z

574 Cherhal F, Cousin F, Capron I (2015) Influence of Charge Density and Ionic Strength on the
575 Aggregation Process of Cellulose Nanocrystals in Aqueous Suspension, as Revealed by Small-
576 Angle Neutron Scattering. Langmuir 31:5596–5602. doi: 10.1021/acs.langmuir.5b00851

577 De France KJ, Hoare T, Cranston ED (2017) Review of Hydrogels and Aerogels Containing
578 Nanocellulose. Chem Mater. doi: 10.1021/acs.chemmater.7b00531

579 Desmaisons J, Boutonnet E, Rueff M, et al (2017) A new quality index for benchmarking of different
580 cellulose nanofibrils. Carbohydr Polym 174:318–329. doi: 10.1016/j.carbpol.2017.06.032

581 Dufresne A (2012) Nanocellulose: From Nature to High Performance Tailored Materials. Walter de
582 Gruyter, Berlin

583 Elazzouzi-Hafraoui S, Nishiyama Y, Putaux J-L, et al (2008) The Shape and Size Distribution of
584 Crystalline Nanoparticles Prepared by Acid Hydrolysis of Native Cellulose. Biomacromolecules
585 9:57–65. doi: 10.1021/bm700769p

586 Elazzouzi-Hafraoui S, Putaux J-L, Heux L (2009) Self-assembling and Chiral Nematic Properties of
587 Organophilic Cellulose Nanocrystals. J Phys Chem B 113:11069–11075. doi:
588 10.1021/jp900122t

589 Foster EJ, Moon RJ, Agarwal UP, et al (2018) Current characterization methods for cellulose
590 nanomaterials. Chem Soc Rev 47:2609–2679. doi: 10.1039/C6CS00895J

591 Fumagalli M, Sanchez F, Boisseau SM, Heux L (2013) Gas-phase esterification of cellulose nanocrystal
592 aerogels for colloidal dispersion in apolar solvents. Soft Matter 9:11309. doi:
593 10.1039/c3sm52062e

594 Gawryla MD, van den Berg O, Weder C, Schiraldi DA (2009) Clay aerogel/cellulose whisker
595 nanocomposites: a nanoscale wattle and daub. J Mater Chem 19:2118. doi:
596 10.1039/b823218k

597 Gibson LJ, Ashby MF (1999) Cellular Solids: Structure and Properties. Cambridge University Press,
598 Cambridge

599 Gupta P, Singh B, Agrawal AK, Maji PK (2018) Low density and high strength nanofibrillated cellulose
600 aerogel for thermal insulation application. Mater Des 158:224–236. doi:
601 10.1016/j.matdes.2018.08.031

602 Habibi Y, Lucia LA, Rojas OJ (2010) Cellulose Nanocrystals: Chemistry, Self-Assembly, and
603 Applications. Chem Rev 110:3479–3500. doi: 10.1021/cr900339w

604 Hoeng F, Denneulin A, Bras J (2016) Use of nanocellulose in printed electronics: a review. Nanoscale
605 8:13131–13154. doi: 10.1039/C6NR03054H

606 Ishida O, Kim D-Y, Kuga S, et al (2004) Microfibrillar carbon from native cellulose. Cellulose 11:475–
607 480. doi: 10.1023/B:CELL.0000046410.31007.0b

608 Jean B, Dubreuil F, Heux L, Cousin F (2008) Structural Details of Cellulose
609 Nanocrystals/Polyelectrolytes Multilayers Probed by Neutron Reflectivity and AFM. Langmuir
610 24:3452–3458. doi: 10.1021/la703045f

611 Jiang F, Hsieh Y-L (2014) Amphiphilic superabsorbent cellulose nanofibril aerogels. J Mater Chem A
612 2:6337–6342. doi: 10.1039/C4TA00743C

613 Jiménez-Saelices C, Seantier B, Cathala B, Grohens Y (2017) Spray freeze-dried nanofibrillated
614 cellulose aerogels with thermal superinsulating properties. Carbohydr Polym 157:105–113.
615 doi: 10.1016/j.carbpol.2016.09.068

616 Jin H, Nishiyama Y, Wada M, Kuga S (2004) Nanofibrillar cellulose aerogels. Colloids Surf Physicochem
617 Eng Asp 240:63–67. doi: 10.1016/j.colsurfa.2004.03.007

618 Jorfi M, Foster EJ (2015) Recent advances in nanocellulose for biomedical applications. J Appl Polym
619 Sci 132:n/a-n/a. doi: 10.1002/app.41719

620 Klemm D, Cranston ED, Fischer D, et al (2018) Nanocellulose as a natural source for groundbreaking
621 applications in materials science: Today's state. Mater Today 21:720–748. doi:
622 10.1016/j.mattod.2018.02.001

623 Klemm D, Kramer F, Moritz S, et al (2011) Nanocelluloses: A New Family of Nature-Based Materials.
624 Angew Chem Int Ed 50:5438–5466. doi: 10.1002/anie.201001273

625 Kriechbaum K, Munier P, Apostolopoulou-Kalkavoura V, Lavoine N (2018) Analysis of the Porous
626 Architecture and Properties of Anisotropic Nanocellulose Foams: A Novel Approach to Assess
627 the Quality of Cellulose Nanofibrils (CNFs). ACS Sustain Chem Eng 6:11959–11967. doi:
628 10.1021/acssuschemeng.8b02278

629 Lavoine N, Bergström L (2017) Nanocellulose-based foams and aerogels: processing, properties, and
630 applications. J Mater Chem A 5:16105–16117. doi: 10.1039/C7TA02807E

631 Lavoine N, Desloges I, Dufresne A, Bras J (2012) Microfibrillated cellulose – Its barrier properties and
632 applications in cellulosic materials: A review. Carbohydr Polym 90:735–764. doi:
633 10.1016/j.carbpol.2012.05.026

634 Martin C, Jean B (2014) Nanocellulose/polymer multilayered thin films: tunable architectures
635 towards tailored physical properties. Nord Pulp Pap Res J 29:19–30. doi: 10.3183/npprj-2014-
636 29-01-p019-030

637 Martoïa F, Cochereau T, Dumont PJJ, et al (2016) Cellulose nanofibril foams: Links between ice-
638 templating conditions, microstructures and mechanical properties. Mater Des 104:376–391.
639 doi: 10.1016/j.matdes.2016.04.088

640 Mueller S, Sapkota J, Nicharat A, et al (2015) Influence of the nanofiber dimensions on the properties
641 of nanocellulose/poly(vinyl alcohol) aerogels. J Appl Polym Sci 132:. doi: 10.1002/app.41740

642 Munier P, Gordeyeva K, Bergström L, Fall AB (2016) Directional Freezing of Nanocellulose Dispersions
643 Aligns the Rod-Like Particles and Produces Low-Density and Robust Particle Networks.
644 Biomacromolecules 17:1875–1881. doi: 10.1021/acs.biomac.6b00304

645 Naderi A, Lindström T, Sundström J (2015) Repeated homogenization, a route for decreasing the
646 energy consumption in the manufacturing process of carboxymethylated nanofibrillated
647 cellulose? Cellulose 22:1147–1157. doi: 10.1007/s10570-015-0576-4

648 Nechyporchuk O, Belgacem MN, Bras J (2016) Production of cellulose nanofibrils: A review of recent
649 advances. Ind Crops Prod 93:2–25. doi: 10.1016/j.indcrop.2016.02.016

650 Nguyen BN, Cudjoe E, Douglas A, et al (2016) Polyimide Cellulose Nanocrystal Composite Aerogels.
651 Macromolecules 49:1692–1703. doi: 10.1021/acs.macromol.5b01573

652 Osorio DA, Seifried B, Moquin P, et al (2018) Morphology of cross-linked cellulose nanocrystal
653 aerogels: cryo-templating versus pressurized gas expansion processing. J Mater Sci 53:9842–
654 9860. doi: 10.1007/s10853-018-2235-2

655 Podsiadlo P, Sui L, Elkasabi Y, et al (2007) Layer-by-Layer Assembled Films of Cellulose Nanowires
656 with Antireflective Properties. Langmuir 23:7901–7906. doi: 10.1021/la700772a

657 Ravikovitch PI, Neimark AV (2001) Characterization of Micro- and Mesoporosity in SBA-15 Materials
658 from Adsorption Data by the NLDFT Method. J Phys Chem B 105:6817–6823. doi:
659 10.1021/jp010621u

660 Revol J-F, Bradford H, Giasson J, et al (1992) Helicoidal self-ordering of cellulose microfibrils in
661 aqueous suspension. Int J Biol Macromol 14:170–172. doi: 10.1016/S0141-8130(05)80008-X

662 Robitzer M, Renzo FD, Quignard F (2011) Natural materials with high surface area. Physisorption
663 methods for the characterization of the texture and surface of polysaccharide aerogels.
664 Microporous Mesoporous Mater 140:9–16. doi: 10.1016/j.micromeso.2010.10.006

665 Rudaz C, Courson R, Bonnet L, et al (2014) Aeropectin: Fully Biomass-Based Mechanically Strong and
666 Thermal Superinsulating Aerogel. Biomacromolecules 15:2188–2195. doi:
667 10.1021/bm500345u

668 Sacui IA, Nieuwendaal RC, Burnett DJ, et al (2014) Comparison of the Properties of Cellulose
669 Nanocrystals and Cellulose Nanofibrils Isolated from Bacteria, Tunicate, and Wood Processed
670 Using Acid, Enzymatic, Mechanical, and Oxidative Methods. ACS Appl Mater Interfaces
671 6:6127–6138. doi: 10.1021/am500359f

672 Sehaqui H, Zhou Q, Berglund LA (2011) High-porosity aerogels of high specific surface area prepared
673 from nanofibrillated cellulose (NFC). Compos Sci Technol 71:1593–1599. doi:
674 10.1016/j.compscitech.2011.07.003

675 Trache D, Hussin MH, Haafiz MKM, Thakur VK (2017) Recent progress in cellulose nanocrystals:
676 sources and production. Nanoscale 9:1763–1786. doi: 10.1039/C6NR09494E

677 Tripathi A, Tardy BL, Khan SA, et al (2019) Expanding the upper limits of robustness of cellulose
678 nanocrystal aerogels: outstanding mechanical performance and associated pore compression
679 response of chiral-nematic architectures. J Mater Chem A. doi: 10.1039/C9TA03950C

680 Wei H, Rodriguez K, Renneckar S, J. Vikesland P (2014) Environmental science and engineering
681 applications of nanocellulose-based nanocomposites. Environ Sci Nano 1:302–316. doi:
682 10.1039/C4EN00059E

683 Yang X, Cranston ED (2014) Chemically Cross-Linked Cellulose Nanocrystal Aerogels with Shape
684 Recovery and Superabsorbent Properties. Chem Mater 26:6016–6025. doi:
685 10.1021/cm502873c

686 Zhao S, Malfait WJ, Guerrero-Alburquerque N, et al (2018) Biopolymer Aerogels and Foams:
687 Chemistry, Properties, and Applications. Angew Chem Int Ed 57:7580–7608. doi:
688 10.1002/anie.201709014

689 Zhao Y, Li J (2014) Excellent chemical and material cellulose from tunicates: diversity in cellulose
690 production yield and chemical and morphological structures from different tunicate species.
691 Cellulose 21:3427–3441. doi: 10.1007/s10570-014-0348-6

692